Additional stratospheric NO_x production by relativistic electron precipitation during the 2004 spring NO_x descent event.

Mark A. Clilverd[1], Annika Seppälä[2], Craig J. Rodger[3], Martin G. Mlynczak[4], and Janet U. Kozyra[5]

Abstract. We analyze in detail the February 2004 GOMOS NO_2 observations in the northern polar latitudes during the spring time descent of NO_x from the mesosphere into the stratosphere. We combine GOMOS observations with SABER-observed NO 5.3 μm radiated power, and an AARDDVARK derived radio wave index (RWI) to describe the impact of the 11 February geomagnetic storm. Energetic electron precipitation generated some additional NO_x, supplementing the original amounts that were already descending. At altitudes 50-70 km GOMOS observations of NO_2 showed a delayed response to the geomagnetic storm, with NO_2 being generated three days after the start of the storm. The delayed response and duration of NO_2 production was found to be consistent with the increase in the flux of relativistic electrons measured by GOES at geostationary orbit, and by POES through relativistic electron contamination of the >16 MeV proton channel. Using the SIC model we found that a good fit to the observed NO_2 mixing ratios at the peak of the geomagnetic storm effect was produced by a mono-energetic 1.25 MeV electron beam with a flux of ~0.3×10^6 el.cm^{-2}sr^{-1}s^{-1}keV^{-1} or with a 'hard' electron spectra taken from Gaines et al. [1995] but with fluxes enhanced by a factor of 15, i.e., 8 x 10^4 el.cm^{-2}sr^{-1}s^{-1} for 2-6 MeV. Prior to the storm the descending NO_2 had average mixing ratio values of ~150 ppbv. The geomagnetic storm-induced REP event doubled the amount of NO_x descending into the stratosphere to ~300 ppbv after the storm.

1. Introduction

During the Arctic winter 2003-2004 several satellite and ground-based experiments observed enhanced concentrations of NO_x descending from mesospheric altitudes. As a consequence of the enhanced levels of NO_x reaching the stratosphere there was a related decrease in the levels of spring-time ozone at 40 km altitudes [Randall et al., 2005]. Winter-time polar odd nitrogen, NO_x ($NO + NO_2$), can be produced in the thermosphere and the mesosphere by energetic particle precipitation [Brasseur and Solomon, 2005]. During periods of efficient vertical transport the NO_x can descend to the stratosphere [Siskind, 2000]. In the upper mesosphere the NO_x is mainly in the form of NO. As the NO descends below 70 km it is converted to NO_2 [Solomon et al., 1982; Brasseur and Solomon, 2005]. The particular descent of interest here began in January 2004 [Clilverd et al., 2006], and was still observable in May 2004. Randall et al. [2005] analyzed NO_2 concentration data from three long-running solar occultation experiments, SAGE II, POAM III, and HALOE during this period. They reported unprecedented levels of spring-time stratospheric NO_x (~45 km) as a result of the descent. Rinsland et al. [2005] also observed very high NO_x mixing ratios at 40-50 km in February/March 2004 with the ACE experiment, detecting levels as high as 1365 ppbv. The source of the NO_x that was ultimately observed at 45 km in May 2004 is still open to debate [Clilverd et al., 2007]. In this work we aim to identify additional contributions to the stratospheric NO_x produced by a geomagnetic storm in February 2004.

Clilverd et al. [2006, 2007] used radio wave data that was sensitive to the ionization of NO_x at 70-90 km altitudes to show that the initial source for the NO_x observed in January 2004 was likely to be in the auroral zones in the thermosphere, and not a result of in situ production in the mesosphere. The data showed that the descent of the NO_x began on 11/12 January 2004, a few days after the end of the stratospheric warming event at the end of December 2003. Seppälä et al. [2007a] used GOMOS NO_2 observations during the polar night to investigate the cause of the descending NO_x observed throughout the winter, November 2003 – March 2004. They concluded that the Halloween solar proton events that occurred in late-October 2003 produced significant levels of NO_2 during November and December 2003, but that a source at thermospheric altitudes was the most likely cause of the NO_2 observed decending in January 2004. However, Seppälä et al. [2007a] also suggested that a further enhancement of NO_x occurred in mid-February 2004 adding to the NO_x that was already descending. In this paper we analyse in detail the period in mid-February 2004 with a view to determining the contribution to the NO_x that was produced by processes driven by the 11 February geomagnetic storm, in addition to that already descending from higher altitudes.

Using the Sodankylä Ion and Neutral Chemistry model (SIC) Turunen et al. [2008] generated NO_2 concentration profiles from four separate particle precipitation mechanisms: solar proton events, auroral electron precipitation, long-lasting relativistic electron precipitation (REP), and REP microbursts. In comparing the SIC results with GOMOS observations from the northern hemisphere polar winter 2003-2004 Turunen et al. [2008] concluded that the mid-February enhancement of NO_2 had the altitude profile characteristics of REP-generation possibly involving an energy spectrum that contained >1 MeV electron fluxes. However, Turunen et al. [2008] did not identify any link to geomagnetic activity, nor what likely electron precipitation fluxes were required to reproduce the GOMOS observations.

In this study we analyze the February 2004 period in detail, concentrating on the GOMOS NO_2 observations in the northern polar latitudes. We combine additional datasets to further describe the impact of the mid-February geomagnetic activity, including the SABER-observed NO 5.3 μm radiated power, and the AARDDVARK-derived radio wave index. We determine the characteristics of the geomagnetic activity that lead to the generation of enhanced NO_2 in the altitude range 40-70 km, and use the SIC model to approximately determine the energy spectrum and flux required to generate the enhanced NO_2 observed. Finally, we determine the relative impact of the geomagnetic storm-induced REP on NO_2 concentration levels in comparison with the descending NO_2 that was first observed on 11/12 January 2004.

2. Event conditions

This study concentrates on the atmospheric effects of energetic particle precipitation during a geomagnetic storm. The event conditions are shown in Figure 1, which shows solar wind conditions, and geomagnetic activity during February 2004. The solar wind shows a sharp increase in density (>20 protons cm^{-3}) on 11 February 2004, followed shortly afterward by a period of high (>600 km s^{-1}) solar wind speed. Although the density increase subsides quickly, the high solar wind speed continues until 16 February, gradually returning to non-disturbed levels (~400 km s^{-1}) by 21 February. Dotted vertical lines on 11 and 16 February 2004 in Figure 1 indicate the beginning and recovery phase of the storm. These dates are also indicated on further figures in this paper for easy comparison.

Prior to the storm there was a period of relatively low solar wind speed lasting >1 day, which is consistent with a pre-storm 'calm' [Clilverd et al., 1993; Borovsky and Steinberg, 2006] and thus suggests that this event may be driven by a coronal interaction region (CIR) rather than an incident coronal mass ejection (ICME). Additional evidence for a CIR-driven event come from the observation that February 2004 is during the declining phase of the 11-year solar cycle, and the event has a 27-day repeating occurrence pattern. Further, in geomagnetic terms the storm that occurred on 11-15 February produced only moderate Kp levels (Kp~4-6), while D_{st} achieved <-100 nT only for a short period, and no increase in proton fluxes occurred during the geomagnetic storm (not shown). All of these phenomena are suggestive of a CIR-driven event rather than CME [Tsurutani et al., 2006; Borovsky and Denton, 2006]. However, we note here that the atmospheric affects observed by GOMOS as a result of this CIR-driven event should be considered as an extreme event as no similar NO_2 enhancements have been found in the GOMOS 2002-2007 summary data, other than from solar proton events [Seppälä et al., 2007b].

3. Experimental setup

In this paper we use NO_2 measurements from the GOMOS stellar occultation instrument [Bertaux et al., 2000; Bertaux et al., 2004; Kyrolä et al., 2004], on board the Envisat satellite, to investigate the signatures of NO_x descent in January/February 2004. GOMOS has the advantage over previous satellite observations of the descent of NO_x into the stratosphere in being able to measure NO_2 at altitudes up to 70 km, and in the dark polar night conditions well inside the polar vortex [Hauchecorne et al., 2005, Kyrölä et al., 2006]. For this study we use GOMOS dark limb (night-time) measurements from the Northern Hemisphere (GOPR version 6.0c or later) from occultations where the star temperature was ≥6800 K. Night-time measurements of NO_2 are a good tracer for NO_x in the stratosphere and the lower mesosphere, but not at higher altitudes where NO_x is mainly in the form of NO and the abundance of NO_2 is very low [Brasseur and Solomon, 2005]. The GOMOS data used in this study were averaged over geographic latitudes 59-80°N. We use this latitude range in order to take advantage of the same GOMOS high temperature stars throughout as much of the February 2004 period as possible. This provides data from the polar region which contains the polar vortex (>60°N for a well developed vortex), and which also correspond to a geomagnetic latitude range from L>2.8, i.e., the outer radiation belt. In some cases we restrict the latitude band to 65-75°N, with a median latitude of 70-71°N, in order to compare the GOMOS results with ion and neutral chemistry model runs at 70°N, and to maintain a consistent number of stars in the analysis throughout the study period. These geographic latitudes correspond to an *L*-shell range of *L*>3.8.

To investigate the variation of high altitude NO during February we use data from the SABER instrument. SABER is a 10 channel limb-scanning radiometer flying on the NASA TIMED satellite, described by Russell et al. [1999]. The primary objective of SABER is to quantify the thermal structure and energy balance of the mesosphere and lower thermosphere. Every 53 s SABER scans the Earth's limb from 400 km tangent height to a height equivalent to 20 km below the hard Earth surface, simultaneously recording profiles of radiance (W cm^{-2} sr^{-1}) in each spectral channel. The instrument continuously scans the Earth limb, recording approximately 1600 profiles of limb radiance per channel per day. The spectral coverage of the instrument is from 1.27 to 15.4 μm [Mlynczak et al., 2005]. Of particular interest for this study is the nighttime auroral 5.3 μm limb emission, and it changes promptly due to increases in NO, temperature, and also atomic oxygen. The data shown in this study is an average of the power radiated by NO in the latitude band 52-90°N – which is the SABER 'high latitude' data product of interest to us here. This geographic latitude range covers the geomagnetic *L*-shell range from *L*>2.1.

One of the few experimental techniques which can probe the ionization at altitudes between the GOMOS and SABER observations uses very low-frequency (VLF) electromagnetic radiation, trapped between the lower ionosphere and the Earth [Barr et al., 2000]. The nature of the received radio waves is largely determined by propagation between these boundaries [e.g., Cummer, 2000], termed "subionospheric propagation". Here we use the AARDDVARK-derived radio wave index (RWI) which describes the variation in propagation conditions for a narrow band subionospheric transmitter (call sign NRK, 64ºN, 22ºW, *L*=5.6, 37.5 kHz) located in

Iceland and received at a receiver located at Ny Ålesund, Svalbard (79ºN, 11ºE, *L*=18.3). Because of the geographic latitude and geomagnetic latitude of this path the propagation conditions are influenced by both the polar vortex and the outer radiation belt, and the path passes through the footprints of geostationary orbits as discussed later in section 4. Any change in the levels of either NO concentration, or ionization rates due to particle precipitation, in the 70-90 km altitude range can be identified in the RWI [Clilverd et al., 2007]. The Ny Ålesund site is part of the Antarctic-Arctic Radiation-belt Dynamic Deposition VLF Atmospheric Research Konsortia (AARDDVARK) - see Clilverd et al. [2008] for more details.

Radiation belt particle data is provided by instruments onboard the Geostationary Operational Environmental Satellite (GOES) and Polar Operational Environmental Satellite (POES) Program spacecraft, which are a cooperative effort between NASA and the National Oceanic and Atmospheric Administration (NOAA). The Space Environment Monitor instrument onboard GOES-11 provides 1-min >2 MeV electron fluxes at a nominal fixed *L*-shell of *L*=6.6. The GOES >2 MeV channel primarily responds to trapped outer-zone particles. In practice the geostationary orbit is not at a constant *L*, and so we use to daily average to compensate for the factor of ~5 variation during a normal "quiet-time" orbit. The Polar Orbiting Environmental Satellites (POES) (formerly known as TIROS for Television and InfraRed Observation Satellite) carry the Space Environment Monitor-2 instrument, which observes trapped and precipitating (loss-cone) electrons and protons. In this study we make use of measurements from the POES spacecraft NOAA-15, 16 and 17. As POES are located in polar orbits, they sweep through a range of *L*-shells, sampling both the inner and outer radiation belts. POES instruments measure trapped and loss cone electron integral fluxes for energy thresholds of >30-, >100- and >300-keV. Here we make use of two POES data products, the POES radiation belt indices (available from http://www.swpc.noaa.gov/ftpdir/lists/bi/old_bi/) and the POES Space Environment Monitor-2 16-second average measurements (available from http://poes.ngdc.noaa.gov/data/avg/). The radiation belt indices are a daily value indicating the ratio of the daily trapped particle counts to their corresponding one-year summed average for each energy channel. The indices are subdivided by L to provide inner ($L < 2.0$), slot ($2.0 \leq L < 2.5$), and outer ($L \geq 2.5$) radiation belt indices.

The POES Space Environment Monitor-2 suite includes a >300 keV loss-cone telescope and an omnidirectional proton integral energy channel with energy threshold >16 MeV which responds to trapped >0.8 MeV electrons as a "contaminant" in the absence of any significant proton fluxes [Sandanger et al., 2007]. We use the 16-second average measurements from the proton integral energy channel to detect trapped relativistic electrons, as there was no solar proton event in this period. The relative detection efficiency of the POES >16 MeV proton channel is 50% for 1.5 MeV electrons and climbs to 100% for 2 MeV electrons [Sandanger et al., 2007], and as such this data is a very useful representation of trapped relativistic electron populations (outside of solar proton events). As the fluxes are being measured at low altitudes they represent a measurement of particles closer to the loss-cone (smaller pitch angles) than the fluxes measured by GOES. So, an increase in the POES omnidirectional detector does indicate when particles have been scattered from near-equatorial pitch angles to closer to the loss-cone, which is consistent with the hypothesis that precipitation is likely to be occurring.

4. Results

In Figure 2 we show a composite picture which combines data from all three experimental techniques during the period January-February 2004. The upper panel shows the daily average NO radiated power from SABER in the northern polar region (52-90°N) in the altitude range 100-200 km, starting from 16 January 2004. The values obtained during January and February varied from 1-7.6 $\times 10^{10}$ W with high levels observed over 16-27 January, and 11-16 February. The start of the first period of enhanced NO radiated power was not captured in the SABER observations. However, the second period is clearly associated with the geomagnetic storm that began on 11 February, and lasted as long as the period of high solar wind speeds, finishing on 15 February. As this change is in step with the 15 μm power for SABER CO_2 data (not shown) we conclude that the NO radiated power increase is likely to be due to storm-induced changes in temperature, rather than an increase in NO due to ionization from low-energy electron precipitation. The middle panel shows the daily AARDDVARK RWI, values varied from -15 to 5 dB during January and February, with an extended period of high levels (denoting enhanced ionospheric ionization levels in the altitude range 70-90 km) from 11 January – 5 February, and then a second period from 11-19 February. The first period of enhanced RWI has been associated with the ionization of descending NO_x by Lyman-α as a result of strong vertical descent associated with a strengthening of the underlying polar vortex [Clilverd et al., 2006, 2007]. The second period of enhanced RWI is co-incident with the 11-16 February geomagnetic storm, although lasting longer than the period of high solar wind speed, and peaking in magnitude at the time that the SABER event finishes.

The bottom panel of Figure 2 shows the daily averaged GOMOS nighttime NO_2 mixing ratios from 30-70 km and 59-80°N. The average mixing ratios range from 0 to 600 ppbv during January and February 2004, with a gradually descending enhancement of NO_x starting at around 70 km on 11 January reaching ~45 km by the end of February. The origin of this descending feature has been ascribed to auroral-altitude (>90 km) NO_x [Clilverd et al., 2007] descending because of strong vertical transport of subsiding polar air [Randall et al., 2005]. The enhancement of NO_2 weakens after 5 February, but is strongly enhanced over a large range of altitudes from 14-19 February coincident with, and following, the geomagnetic storm shown in Figure 1. Seppälä et al. [2007a] and Turunen et al. [2008] identified this increase in NO_2 in the GOMOS data as being due to in-situ generation of NO_x by energetic electron precipitation, suggesting relativistic electron precipitation as the most likely source because of the altitude at which the NO_2 was generated. In this paper we study this period in detail and attempt to quantify the contribution of the energetic electron precipitation to the NO_x levels that were eventually observed at 40 km by Randall et al. [2005] and Rinsland et al. [2005].

One interesting difference in the geomagnetic storm as seen in the SABER NO radiated power, the AARDDVARK RWI, and the GOMOS NO_2 data is in the timing of the event at the different altitudes that the datasets represent. At altitudes >100 km the storm effect is observed by SABER from 11-16 February. However, at 50-70 km the storm effect is seen by GOMOS from 14-19 February. Starting later and finishing later than the SABER event. The 70-90 km RWI also confirms the later finish date at altitudes <100 km. Of particular interest to this paper is why the NO_2 generated at 50-70 km altitudes is so delayed with respect to the storm start.

Figure 3 gives an insight into why the two altitudes respond at such different times. The upper panel of the figure shows the variation of the POES outer radiation belt (*L*>2.5) daily index for >30 keV electrons, and a daily average of the GOES >2 MeV trapped electron fluxes (*L*=6.6). Precipitating 30 keV electrons produce ionization at >90 km altitudes [Rees, 1989; Turunen et al., 2008], while precipitating 2 MeV electrons produce ionization at >50-km. Thus the POES >30 keV electron index is more useful for comparison with SABER data, while the GOES >2 MeV electron fluxes are more useful for comparison with the GOMOS data. The lower panel of Figure 3 shows the variation of the POES count rates in February 2004 for the ~1.5 MeV onmidirectional detector and the >300 keV loss-cone detector, measured at L=4.5, i.e., in the heart of the outer radiation belt. In both the upper and lower panels we can see that the POES outer radiation belt index and the > 300 keV loss cone counts respond at the beginning of the storm period (11 February), while the GOES >2 MeV trapped fluxes and the POES ~1.5 MeV omnidirectional detector respond later, and peak after, the POES outer radiation belt index and the > 300 keV loss cone counts. We note here that the increase in GOES fluxes indicates an increase in trapped fluxes which may lead to higher precipitating fluxes. The low-atitude POES omnidirectional detector measurements, which also show an increase, are consistent with this hypothesis.

In Figure 4 we show POES data plotted as a function of *L*-shell versus date in February 2004. The 16-second average measurements from all 3 POES spacecraft are processed to create mean flux measurements in bins which are 3-hours and 0.25 *L* wide, with measurements taken from inside the South Atlantic Magnetic Anomaly removed. The upper panel shows values from the POES >16 MeV omnidirectional proton channel which responds to relativistic electrons. We follow the approach of previous authors in describing this as a ~1.5 MeV electron channel [Sandanger et al., 2007], although as noted above the detection efficiency of this proton channel for relativistic electrons is energy dependent. The geomagnetic storm of 11 February produces very low fluxes of relativistic electron contamination initially, but high relativistic electron fluxes at *L*>4 from 14-21 February, consistent with the period of GOMOS NO_2 production. The middle panel shows the POES >300 keV loss cone electron flux, while the lower panel shows that the POES >30 keV loss cone electron flux. The loss cone fluxes undergo a sudden enhancement at L>4 on 11 February, lasting until 16 February, contiguous with high solar wind speeds during the geomagnetic storm, and SABER NO radiated power observations. Thus from Figures 3 and 4 we conclude that enhanced fluxes of trapped relativistic electrons are generated at L>4 and as far out as L~7 - as the effect is seen clearly in the GOES data at L=6.6. The generation is delayed by ~3-4 days in respect of the start of the storm, which is consistent with acceleration of seed populations of low energy electrons by wave-particle interactions or radial diffusion, and consistent with CIR-driven storms [Tsurutani et al., 2006]. Although the loss-cone measurements at >30 keV and >300 keV do not show any significant enhancements from 16-19 February, the enhancement of the quasi-trapped >1.5 MeV fluxes is consistent with the results from previous studies of this period in suggesting that the increase in GOMOS NO_2 is a result of increased relativistic electron precipitation into the atmosphere [Seppälä et al., 2007a; Turunen et al., 2008].

5. Modeling the REP-generated NO_x

The detailed impact of the geomagnetic storm of 11-16 February 2004 on the NO_2 altitude profiles in the latitude range 65°-75°N, which is where the maximum NO_2 enhancement was observed, is shown in Figure 5. The upper panel identifies three critical periods: before, during, and after the storm. Before the storm, from 1-5 February, the average NO_2 profile is represented by a maximum in mixing ratio at ~55 km, with values of ~150 ppbv. There is little NO_2 below 50 km or above 60 km. During the latter part of the storm, from 15-20 February, the average NO_2 profile is represented by a maximum in mixing ratio between 52 and 56 km, with values of >500 ppbv. There is some NO_2 as low as ~47 km, but significant amounts occur over a larger altitude range than before the storm, up to 65 km in altitude. After the storm, from 25-29 February, the NO_2 profile is represented by a maximum in mixing ratio at ~52 km, with values of ~300 ppbv, but the altitude range over which significant NO_2 occurs has again reduced to ~10 km.

The lower panel shows 2-day averages of the NO_2 mixing ratio (circles) measured at the peak of the descending feature, where the altitude of the measurement is shown by the squares in the same panel. Following a period at the beginning of January, where the mixing ratio values are steadily increasing because of conversion from NO to NO_2 with decreasing altitude [Brasseur and Solomon, 2005], the mixing ratios then remain at a quasi-constant value of ~150 ppbv until 7 February. Between 8 and 13 February there is a gap in the occurrence of measurements in the 65°-75°N latitude range. However, GOMOS observations in Figure 2 show that no immediate effect of the geomagnetic storm on NO_2 is observed at the onset of the storm. During and just after the geomagnetic storm (14-18 Feb) the mixing ratios increase to 600 ppbv before settling back down to ~300 ppbv late in February. The loss of ~200 ppbv of NO_2 at the end of the geomagnetic storm is consistent with the removal of NO_2 into reservoir species such as $ClONO_2$ [von Clarmann et al., 2005; López-Puertas et al., 2005]. Delayed $ClONO_2$ increases were observed by MIPAS instruments following the October 2003 solar proton events as a result of temporal development of active chlorine during the storm, with subsequent buffering into its inactive reservoir ($ClONO_2$) [von Clarmann et al., 2005]. Reactions such as this may account for the observed loss of NO_2 at the end of the geomagnetic storm - loss by photolysis alone seems unable to explain the rapid temporal variability shown.

After 20 February the NO_2 mixing ratios remain at an elevated and quasi-constant level of ~300 ppbv. From these measurements we conclude that in overall terms the geomagnetic storm doubled the amount of NO_x that was descending towards the stratosphere. The low altitude, high latitude, and winter time conditions for this event mean that any loss of NO_x by photolysis is minimal, and the NO_x should be able to survive long enough to descend to low altitudes with the post-storm mixing ratios, which is consistent with the observations of Randall et al. [2005] for April/May 2004 at ~40 km altitudes.

In this section we use the Sodankylä Ion and Neutral Chemistry model (SIC) to investigate what energy spectrum and flux of precipitating electrons are required to generate the altitude profile of NO_2 observed by GOMOS at the peak of the geomagnetic storm effect. The SIC model is a 1-D chemical model designed for ionospheric D-region studies, solving the concentrations of 65 ions, including 29 negative ions, and 15 neutral species at altitudes across 20–150 km. This study makes use of SIC version 6.9.0. A detailed overview of the model was given in *Verronen et al.* [2005], building on original work by *Turunen et al.* [1996] and *Verronen et al.* [2002]. In the SIC model several hundred reactions are implemented, plus additional external forcing due to solar radiation (1–422.5 nm), electron and proton precipitation, and galactic cosmic radiation. Initial descriptions of the model are provided by *Turunen et al.* [1996], with neutral species modifications described by *Verronen et al.* [2002]. Solar flux is calculated with the SOLAR2000 model (version 2.27) [*Tobiska et al.*, 2000]. The scattered component of solar Lyman-*α* flux is included using the empirical approximation given by *Thomas and Bowman* [1986]. The SIC code includes vertical transport [*Chabrillat et al.*, 2002] which takes into account molecular [*Banks and Kockarts*, 1973] and eddy diffusion with a fixed eddy diffusion coefficient profile. The background neutral atmosphere is calculated using the MSISE-90 model [*Hedin*, 1991] and tables given by *Shimazaki* [1984]. Transport and chemistry are advanced in intervals of 5 or 15 minutes. While within each interval exponentially increasing time steps are used because of the wide range of chemical time constants of the modeled species.

In reality the method used here was one of iteration, with a general target of keeping assumptions to a minimum. Initially a simple energy spectrum for the electron precipitation is assumed, along with a precipitation flux. Then the altitude-dependent ionization rate is calculated making use of the expressions given by Rees [1989, chapter 3], with effective electron ranges taken from Goldberg and Jackman [1984]. Finally we ran the SIC model with the ionization rates imposed to determine the amount of NO_x that would be generated by that amount of ionization. As a result of this iterative process, we identified that the ionization rate profile from a mono-energetic beam of 1.25 MeV electrons with a flux of 0.3×10^6 el.cm^{-2}sr^{-1}s^{-1}keV^{-1} was able to reproduce the GOMOS observations. Figure 6 shows the ionization rate profile from the final electron beam parameters. The energy of the electrons strongly defines the altitude of the peak ionization rate, although it should be noted that substantial ionization occurs at altitudes above the peak even with a mono-energetic beam, due to scattering on the way through the atmosphere. For comparison we also show the ionization rate profile generated by the spectrum shown in Figure 3 (May 18, 1992, 2247 UT) in Gaines et al. [1995] and discussed in Turunen et al. [2008], but with the fluxes multiplied by a factor of 15. The resultant ionization rate profile is very similar to the mono-energetic beam apart from an increased contribution at ~15 km due to the ~5 MeV electrons in the Gaines et al. spectra.

The concentration of NO_2 in the altitude range 40-70 km is shown in Figure 7. NO_2 was generated by imposing the ionization rates from either the mono-energetic beam of 1.25 MeV electrons, or the enhanced Gaines et al. [1995] spectra, on the SIC calculations made at 70°N, 0°E for 3 days. The SIC NO_2 variation with altitude four days after the ionization period is indicated by the black solid line. In comparison, the largest nighttime GOMOS NO_2 average values from 65°-75°N are shown by the dashed line. The gray line represents the SIC model NO_2 profile without electron precipitation forcing. The GOMOS data during the geomagnetic storm is reasonably modeled by the effects of either the mono-energetic 1.25 MeV electron precipitation, or the 40 times enhanced Gaines spectra, at altitudes 45-60 km. The 1.25 MeV mon-energetic flux of 0.3×10^6 el.cm^{-2}sr^{-1}s^{-1}keV^{-1} produces the peak values of 500 ppbv when taking into account the 150 pbv that was already present prior to the geomagnetic storm.

The estimated fluxes for this event can be put into context by comparing them with satellite measurements of electron precipitation fluxes made during geomagnetic storms. The Gaines et al. [1995] bounce loss cone (BLC) spectra from a storm-time period in 18 May 1992 at 2247 UT gave 5.3 x 10^3 el.cm^{-2}sr^{-1}s^{-1} for 2-6 MeV between L = 3.5 and 4.0. Gaines et al. [1995] showed that these fluxes were larger than the drift loss cone (DLC) fluxes at the same time, i.e., at electron precipitation energies which are capable of reaching ~50 km altitudes the BLC fluxes have been observed to be 200% of the DLC fluxes. Daily average BLC and DLC flux comparisons shown in Gaines et al. [1995] also suggest that they can be about the same at the high energy end (>2 MeV) during storms. Using ~11 years of data the SAMPEX observations of DLC fluxes for 2-6 MeV electrons between L=3 and 4.5 are typically ~10^5 el.cm^{-2}sr^{-1}s^{-1} during long-lived, storm-time, flux enhancements [Baker et al., 2004]. The Gaines x 15 BLC spectra from a flux enhancement event (used in this modeling study) represents ~80% of the DLC flux (>2 MeV) seen by SAMPEX during the storm period studied here [Baker et al., 2004].

6. Summary

During the much discussed descent of polar NO_x in the northern hemisphere spring 2004 [Randall et al., 2005; Rinsland et al., 2005; Clilverd et al., 2006] a geomagnetic storm occurred on 11-16 February 2004 that appeared to generate some additional NO_x, supplementing the original amounts that were already descending. At altitudes >70 km SABER observations and AARDDVARK radio wave data showed an immediate affect of the geomagnetic storm which coincide with either the generation of NO by relatively low energy electron precipitation (~30 keV) or with enhanced temperatures at altitudes >100 km, or both, probably associated with direct input from the solar wind. The enhancement of SABER NO radiated power ended when the solar wind speed fell below 600 kms^{-1} 4-5 days after the start of the storm, but the 70-90 km AARDDVARK radio wave data continued to show a response for a further 4 days, recovering on 19 February.

At altitudes 50-70 km GOMOS observations of NO_2 showed a delayed response to the geomagnetic storm with NO_2 being generated from 14-19 February. The delayed response and duration of NO_2 production was found to be consistent with the increase in the flux of trapped relativistic electrons measured by GOES at geostationary orbit and by POES through relativistic electron contamination of the >16 MeV proton channel. The delayed enhancement of radiation belt relativistic electron fluxes is consistent with the acceleration of seed populations of low energy electrons after the onset of the storm, reaching relativistic energies after several days [Horne, 2002; Horne et al., 2005]. The accelerated electrons are then presumably lost to the atmosphere by particle precipitation mechanisms also driven by the geomagnetic storm [e.g., Rodger et al., 2007]. Using the SIC model we found that a good fit to the observed NO_2 mixing rations at the peak of the geomagnetic storm effect was produced by either a mono-energetic 1.25 MeV electron beam with a flux of $\sim 0.3\times 10^6$ $el.cm^{-2}sr^{-1}s^{-1}keV^{-1}$ or a 15 times enhanced Gaines et al. [1995] bounce loss-cone spectra which gives fluxes of 8 x 10^4 $el.cm^{-2}sr^{-1}s^{-1}$ for 2-6 MeV. The geomagnetic storm that generated this upper stratospheric NO_x was driven by a CIR-type storm with high solar wind speeds, moderate Kp, and a 3-day delayed build up of >2 MeV electron fluxes at geostationary orbit. The NO_x was generated by precipitating electron fluxes that lasted for ~3 days, and our observations suggest that this geomagnetic storm was particularly geo-effective in terms of relativistic electron loss into the atmosphere.

Prior to the storm the descending NO_2 had mixing ratio values of ~150 ppbv. After the storm the descending NO_2 had mixing ratios of ~300 ppbv, which leads us to conclude that the geomagnetic storm-induced REP event doubled the amount of NO_x descending into the stratosphere, in comparison with the original event that started in January 2004. However, during the peak of the relativistic electron precipitation effect the maximum mixing ratios observed were ~500 ppbv. We speculate that part of the observed ~200 ppbv loss of NO_2 at the end of the geomagnetic storm could be caused by the removal of NO_2 into reservoir species such as $ClONO_2$.

Acknowledgments. MAC would like to thank Ms Glenda Harden at BAS for her valuable support in the development of this work. AS thanks the Academy of Finland for their support though the EPPIC project. The authors would like to thank the SABER and GOMOS science teams for useful and informative discussions regarding this work. We are grateful to NASA and the National Oceanic and Atmospheric Administration (NOAA) for the observations provided by the Polar Operational Environmental Satellite (POES) and Geostationary Operational Environmental Satellite Program (GOES) programs.

References

Baker, D. N., S. G. Kanekal, X. Li, S. P. Monk, J. Goldstein and J. L. Burch (2004), An extreme distortion of the Van Allen belt arising from the 'Hallowe'en' solar storm in 2003, *Nature,* 432, 878-881.

Banks, P. M., and G. Kockarts (1973), *Aeronomy*, vol. B, chap. 15, Academic Press.

Barr, R., D. L. Jones, and C. J. Rodger (2000), ELF and VLF Radio Waves, *J. Atmos. Sol. Terr. Phys.*, 62(17-18), 1689-1718.

Bertaux, J. L., E. Kyrölä, and T. Wehr (2000), Stellar occultation technique for atmospheric ozone monitoring: GOMOS on Envisat, *Earth Observation Quarterly*, 67, 17-20.

Bertaux, J. L., et al. (2004), First results on GOMOS/Envisat, *Adv. Space Res.*, 33, 1029-1035.

Borovsky J. E., and J. T. Steinberg (2006), The “calm before the storm” in CIR/magnetosphere interactions: Occurrence statistics, solar wind statistics, and magnetospheric preconditioning, *J. Geophys. Res.,* 111, A07S10, doi:10.1029/2005JA011397.

Borovsky, J. E., and M. H. Denton (2006), Differences between CME-driven storms and CIR-driven storms, *J. Geophys. Res.*, *111*, A07S08, doi:10.1029/2005JA011447.

Brasseur, G., and S. Solomon (2005), *Aeronomy of the Middle Atmosphere*, third ed., D. Reidel Publishing Company, Dordrecht.

Chabrillat, S., G. Kockarts, D. Fonteyn, and G. Brasseur (2002), Impact of molecular diffusion on the CO_2 distribution and the temperature in the mesosphere, *Geophys. Res. Lett.*, 29, 1-4.

Clilverd, M.A., T. D. G. Clark, A. J. Smith, and N. R. Thomson (1993), Observation of a decrease in midlatitude whistler-mode signal occurrence prior to geomagnetic storms, *J. Atmos. Terr. Phys.*, 55, 1479-1485.

Clilverd, M. A., A. Seppälä, C. J. Rodger, P. T. Verronen, and N. R. Thomson (2006), Ionospheric evidence of thermosphere-to-stratosphere descent of polar NO_X, *Geophys. Res. Lett.*, 33, L19811, doi: 10.1029/2006GL026727.

Clilverd, M. A., A Seppälä, C. J. Rodger, N. R. Thomson, J. Lichtenberger, and P. Steinbach (2007), Temporal variability of the descent of high-altitude NOX, *J. Geophys. Res.*, 112, A09307, doi:10.1029/2006JA012085.

Clilverd, M. A., C. J. Rodger, N. R Thomson, J. B. Brundell, Th. Ulich, J. Lichtenberger, N. Cobbett, A. B. Collier, F. W. Menk, A. Seppälä, P. T. Verronen, and E. Turunen (2008), Remote sensing space weather events: the AARDDVARK network, *Space Weather,* Submitted.

Cummer, S. A. (2000), Modeling electromagnetic propagation in the earth-ionosphere waveguide, *IEEE Transactions on Antennas and Propagation*, 48(9), 1420-1429.

Gaines, E., D. Chenette, W. Imhof, C. Jackman, and J. Winningham (1995), Relativistic electron fluxes in May 1992 and their effect on the middle atmosphere, J. Geophys. Res., 100(D1), 1027-1033.

Goldberg, R. A., and C. H. Jackman (1984), Nighttime auroral energy deposition in the middle atmosphere, *J. Geophys. Res*., 89(A7), 5581-5596.

Hauchecorne, A., et al. (2005), First simultaneous global measurements of nighttime stratospheric NO_2 and NO_3 observed by Global Ozone Monitoring by Occultation of Stars (GOMOS)/Envisat in 2003, *J. Geophys. Res.,* 110 (D18): Art. No. D18301.

Hedin, A. E. (1991), Extension of the MSIS Thermospheric model into the middle and lower Atmosphere, *J. Geophys. Res.*, 96, 1159-1172.

Horne, R. B. (2002), The contribution of wave-particle interactions to electron loss and acceleration in the Earth's radiation belts during geomagnetic storms, in *URSI Review of Radio Science 1999-2002*, edited by W.R. Stone, pp. 801-828, Wiley.

Horne, R. B., R. M. Thorne, Y. Y. Shprits, et al. (2005), Wave acceleration of electrons in the Van Allen radiation belts, *Nature*, 437, 227 - 230.

Kyrölä, E., et al. (2004), GOMOS on Envisat: An overview, *Adv. Space Res*., 33, 1020-1028.

Kyrölä, E., et al. (2006), Nighttime ozone profiles in the stratosphere and mesosphere by the Global Ozone Monitoring by Occultation of Stars on Envisat, *J. Geophys. Res.,* 111, D24306, doi:10.1029/2006JD007193.

Lopez-Puertas, M., B. Funke., S. Gil-Lopez, T. von Clarmann., G. P. Stiller, M. Hopfner, S. Kellman., H. Fischer, C. H. Jackman (2005), Observation of NO_X enhancements and ozone depletion in the northern and southern hemispheres after the October-November 2003 solar proton events, *J. Geophys. Res.*, 110 (A9), doi:10.1029/2005JA011050.

Mlynczak, M. G., et al. (2005), Energy transport in the thermosphere during the solar storms of April 2002, *J. Geophys. Res.,* 110, A12S25, doi:10.1029/2005JA011141.

Randall, C. E., et al. (2005), Stratospheric effects of energetic particle precipitation in 2003–2004, *Geophys. Res. Lett.*, 32, L05802, doi:10.1029/2004GL022003.

Rees, M. H., 1989. Physics and chemistry of the upper atmosphere, Cambridge University Press, Cambridge.

Reeves, G.D., et al. 2003. Acceleration and loss of relativistic electrons during geomagnetic storms, *Geophys. Res. Lett,* 30, 1529, doi:10.1029/2002GL016513.

Rinsland, C. P., C. Boone, R. Nassar, K. Walker, P. Bernath, J. C. McConnell, and L. Chiou (2005), Atmospheric Chemistry Experiment (ACE) Arctic stratospheric measurements of NO_x during February and March 2004: Impact of intense solar flares, *Geophys. Res. Lett.*, 32, L16S05, doi:10.1029/2005GL022425.

Rodger, C. J., M A Clilverd, N. R. Thomson, R. J. Gamble, A. Seppälä, E. Turunen, N. P. Meredith, M. Parrot, J. A. Sauvaud, and J.-J. Berthelier (2007), Radiation belt electron precipitation into the atmosphere: recovery from a geomagnetic storm, *J. Geophys. Res.*, 112, A11307, doi:10.1029/2007JA012383.

Russell, J. M., III, M. G. Mlynczak, L. L. Gordley, J. Tansock, and R. Esplin (1999), An overview of the SABER experiment and preliminary calibration results, in Proceedings of the SPIE, 44th Annual Meeting, Denver, Colorado, July 18–23, 3756, pp. 277–288.

Sandanger M., F. Søraas, K. Aarsnes, K. Oksavik, D. S. Evans (2007), Loss of relativistic electrons: Evidence for pitch angle scattering by electromagnetic ion cyclotron waves excited by unstable ring current protons, *J. Geophys. Res.,* 112, A12213, doi:10.1029/2006JA012138.

Seppälä, A., M. A. Clilverd, and C. J. Rodger (2007a), NOX enhancements in the middle atmosphere during 2003-2004 polar winter: Relative significance of solar proton events and the aurora as a source, *J. Geophys. Res.*, D23303, doi:10.1029/2006JD008326.

Seppälä, A., P. T. Verronen, M. A. Clilverd, C. E. Randall, J. Tamminen, V. Sofieva, L. Backman, and E. Kyrölä (2007b), Arctic and Antarctic polar winter NO_x and energetic particle precipitation in 2002–2006, *Geophys. Res. Lett.*, *34*, L12810, doi:10.1029/2007GL029733.

Shimazaki, T. (1984), *Minor Constituents in the Middle Atmosphere (Developments in Earth and Planetary Physics, No 6)*, D. Reidel Publishing Co., Dordrecht, Netherlands.

Solomon S, P. J. Crutzen, R. G. Roble (1982), Photochemical coupling between the thermosphere and the lower atmosphere. 1, Odd nitrogen from 50 to 120 km, *J. Geophys. Res.*, 87, 7206-7220.

Thomas, L., and M. R. Bowman (1986), A study of pre-sunrise changes in negative ions and electrons in the D-region, *Ann. Goephys.*, 4, 219-228.

Tobiska, W. K., T. Woods, F. Eparvier, R. Viereck, L. D. B. Floyd, G. Rottman, and O. R. White (2000), The SOLAR2000 empirical solar irradiance model and forecast tool, *J. Atmos. Terr. Phys.*, 62, 1233-1250.

Tsurutani, B. T., et al. (2006), Corotating solar wind streams and recurrent geomagnetic activity: A review, *J. Geophys. Res.*, *111*, A07S01, doi:10.1029/2005JA011273.

Turunen, E., H. Matveinen, J. Tolvanen, and H. Ranta (1996), D-region ion chemistry model, in *STEP Handbook of Ionospheric Models*, edited by R. W. Schunk, pp. 1-25, SCOSTEP Secretariat, Boulder, Colorado, USA.

Turunen, E., P. T. Verronen , A. Seppälä, C. J. Rodger, M. A. Clilverd, J. Tamminen, C.l-F. Enell, and Th. Ulich (2008), Impact of different precipitation energies on NOx generation during geomagnetic storms, J. Atmos. Sol.-Terr. Phys., In Press.

Verronen, P. T., E. Turunen, Th. Ulich, and E. Kyrölä (2002), Modelling the effects of the October 1989 solar proton event on mesospheric odd nitrogen using a detailed ion and neutral chemistry model, *Ann. Geophys.*, 20, 1967-1976.

Verronen, P. T., A. Seppälä, M. A. Clilverd, C. J. Rodger, E. Kyrölä, C.-F. Enell, Th. Ulich, and E. Turunen (2005), Diurnal variation of ozone depletion during the October-November 2003 solar proton event, *J. Geophys. Res.*, 110(A9), doi:10.1029/2004JA010932.

von Clarmann T., N. Glatthor, M. Höpfner, S. Kellmann, R. Ruhnke, G. P. Stiller, H. Fischer, B. Funke, S. Gil-López, M. López-Puertas (2005), Experimental evidence of perturbed odd hydrogen and chlorine chemistry after the October 2003 solar proton events, *J. Geophys. Res.*, 110, A09S45, doi:10.1029/2005JA011053.

---

[1]M. A. Clilverd, Physical Sciences Division, British Antarctic Survey (NERC), High Cross, Madingley Road, Cambridge CB3 0ET, England, U.K. (e-mail: macl@bas.ac.uk)
[2]A. Seppälä, British Antarctic Survey (NERC), High Cross, Madingley Road, Cambridge CB3 0ET, England, U.K. and Finnish Meteorological Institue, P.O. Box 503, FI-00101 Helsinki, Finland (email: annika.seppälä@fmi.fi)
[3]C. J. Rodger, Department of Physics, University of Otago, P.O. Box 56, Dunedin, New Zealand. (email: crodger@physics.otago.ac.nz)
[4]M. G. Mlynczak, NASA Langley Research Center, Hampton, VA 23681-0001, USA. (email: martin.g.mlynczak@nasa.gov)
[5]J. U. Kozyra, Atmospheric, Oceanic and Space Sciences Dept., College of Engineering, University of Michigan, 2455 Hayward, Ann. Arbor, MI 48109-2143, USA. (email: jukozyra@umich.edu)

(Received N x, 2008; N x 27, 2008;

accepted N x, 2008.)

Figures

Figure 1. Upper panel: The variation in solar wind speed and density during February 2004. Upper middle panel: The variation of the B_Z component of the solar wind during February 2004. Lower middle panel: 3-hourly Kp index values, with disturbed times (Kp>5) shown in red, moderately disturbed (4<Kp<5) in green, and quiet times (Kp<4) in blue. Lower panel: The variation in D_{st} (black line) and GOES proton flux units (>10 MeV protons $cm^{-2}s^{-1}sr^{-1}$) in red. A significant geomagnetic disturbance can be seen starting 11 February 2004 lasting until 16 February. There is no equivalent proton enhancement (not shown).

Figure 2. A composite figure showing (top) the SABER NO 5.3 μm radiated power (100-200 km), (middle) AARDDVARK radio wave index (RWI, 70-90 km), and (bottom) average 59-80° latitude GOMOS NO_2 mixing ratio (30-70 km) during January and February 2004. Enhanced NO_2, RWI, and NO can be seen from 11 January 2004, followed by another enhancement from 11 February 2004. Recovery to the second enhancement takes ~5 days at >100 km (denoted by the dashed vertical lines), but continues to the end of the plot window at ~50 km.

Figure 3. Upper panel: The variation of the POES outer radiation belt index (>30 keV electrons) and the daily averaged GOES-12 >2 MeV electron flux in February 2004. The outer radiation belt index shows an immediate response to the geomagnetic storm on 11 February, peaking on 12 February, while the >2 MeV fluxes gradually start to increase 2 days after onset of the geomagnetic storm, peaking on 18 February. Lower panel: The variation of the POES >1.5 MeV omnidirectional detector and the >300 keV loss-cone detector for L=4.5 during February 2004.

Figure 4. Upper panel: The POES >16 MeV proton channel during February 2004 which we use here to identify relativistic electrons (>0.8 MeV). The geomagnetic storm produces high relativistic electron fluxes at *L*>4 from 14-21 February, consistent with the period of GOMOS NO_2 production. Middle panel: The POES >300 keV loss cone electron flux variation with *L*-shell. Lower panel: The POES >30 keV loss cone electron flux variation with *L*-shell. The fluxes show a sudden enhancement on 11 February, lasting until 16 February, contiguous with high solar wind speeds during the geomagnetic storm, and SABER NO 5.3 μm radiated power observations. All panels show values in counts/s.

Figure 5. Upper panel: Showing the variation in the latitude range 65-75°N of the NO_2 mixing ratio with altitude during three selected periods during February 2004. The blue line represents observations made before the onset of the geomagnetic storm period, the green line is during the geomagnetic storm, and the red line is after the end of the storm. Lower panel: The 2-day average mixing ratio (circles) at the peak of the descending NO_x feature (squares represent the altitude of the peak), measured during January and February. There was a gradual increase in mixing ratio from low levels at the start of January, leveling off at ~150 ppbv between 22 January – 05 February, then increasing from 14 February, leveling off again at ~300 ppbv by the end of the month, consistent with the upper panel.

Figure 6. The ionization rate generated by a mono-energetic beam of 1.25 MeV electrons, and a 15 x Gaines et al. [1995] storm-time spectra, imposed on the SIC model to reproduce the observed NO_2 mixing ratios that occurred during the geomagnetic storm of 15-20 February 2004.

Figure 7. The altitude variation of the NO_2 densities observed by GOMOS during the maximum effect of the geomagnetic storm (dashed line) compared with the

calculated SIC quiet-time NO_2 concentrations (grey line) and the results from the mono-energetic 1.25 MeV REP forcing with a flux of 0.3×10^6 el.cm^{-2}sr^{-1}s^{-1}keV^{-1} (black line), and the enhanced Gaines et al. [1995] spectra (dot-dashed line). Good agreement is obtained between the GOMOS data and the SIC results using these levels of REP..

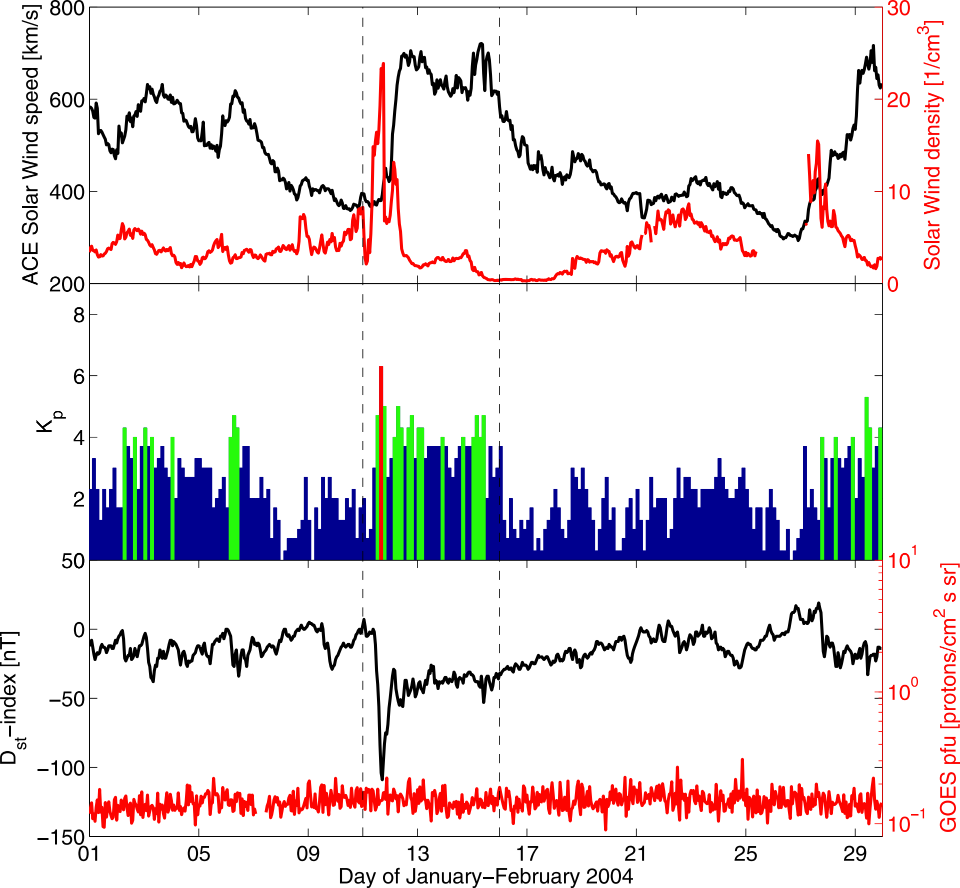

ACE Solar Wind speed [km/s]
Solar Wind density [1/cm^3]
800
600
400
200
30
20
10
0
K$_p$
8
6
4
2
50
0
−50
−100
−150
D$_{st}$−index [nT]
GOES pfu [protons/cm^2 s sr]
10^1
10^0
10$^{−1}$
01
05
09
13
17
21
25
29
Day of January−February 2004

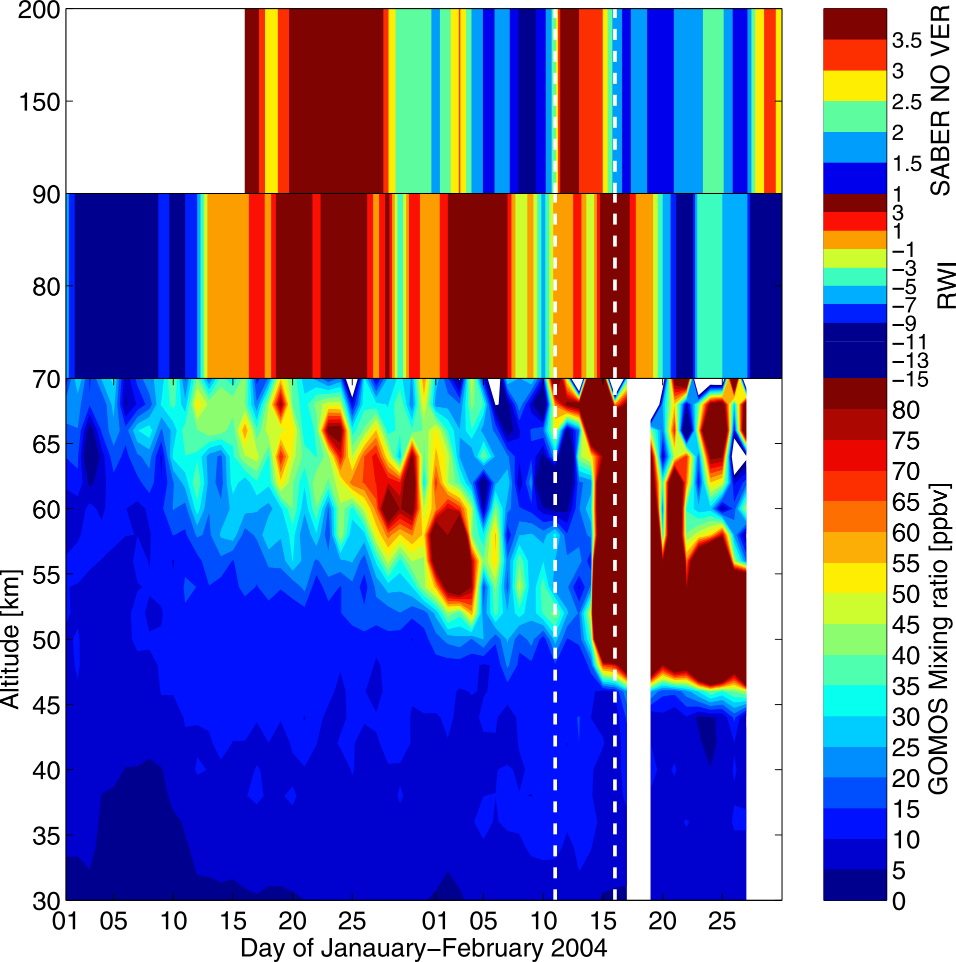

Altitude [km]
Day of Janauary–February 2004
01 05 10 15 20 25 01 05 10 15 20 25
30 35 40 45 50 55 60 65 70 80 90 150 200
SABER NO VER
3.5 3 2.5 2 1.5 1
RWI
3 1 −1 −3 −5 −7 −9 −11 −13 −15
GOMOS Mixing ratio [ppbv]
80 75 70 65 60 55 50 45 40 35 30 25 20 15 10 5 0

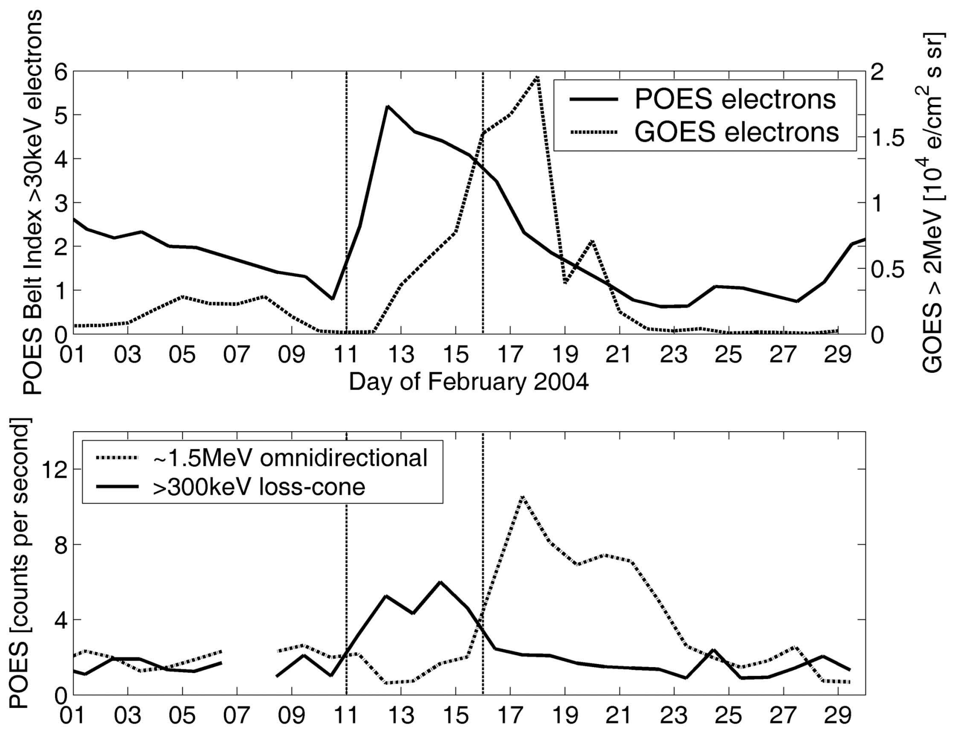

POES Belt Index >30keV electrons
GOES > 2MeV [10^4 e/cm^2 s sr]
POES electrons
GOES electrons
6
5
4
3
2
1
0
2
1.5
1
0.5
0
01 03 05 07 09 11 13 15 17 19 21 23 25 27 29
Day of February 2004
POES [counts per second]
~1.5MeV omnidirectional
>300keV loss-cone
12
8
4
0
01 03 05 07 09 11 13 15 17 19 21 23 25 27 29

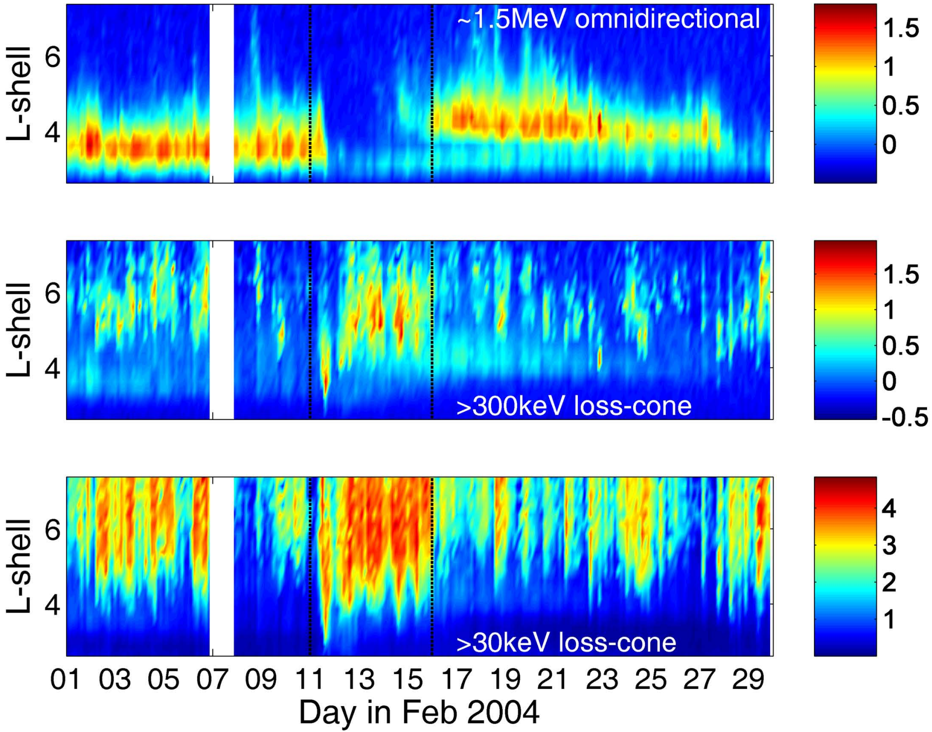
~1.5MeV omnidirectional
>300keV loss-cone
>30keV loss-cone
L-shell
Day in Feb 2004
01 03 05 07 09 11 13 15 17 19 21 23 25 27 29
1.5
1
0.5
0
-0.5
4
3
2
1
6
4

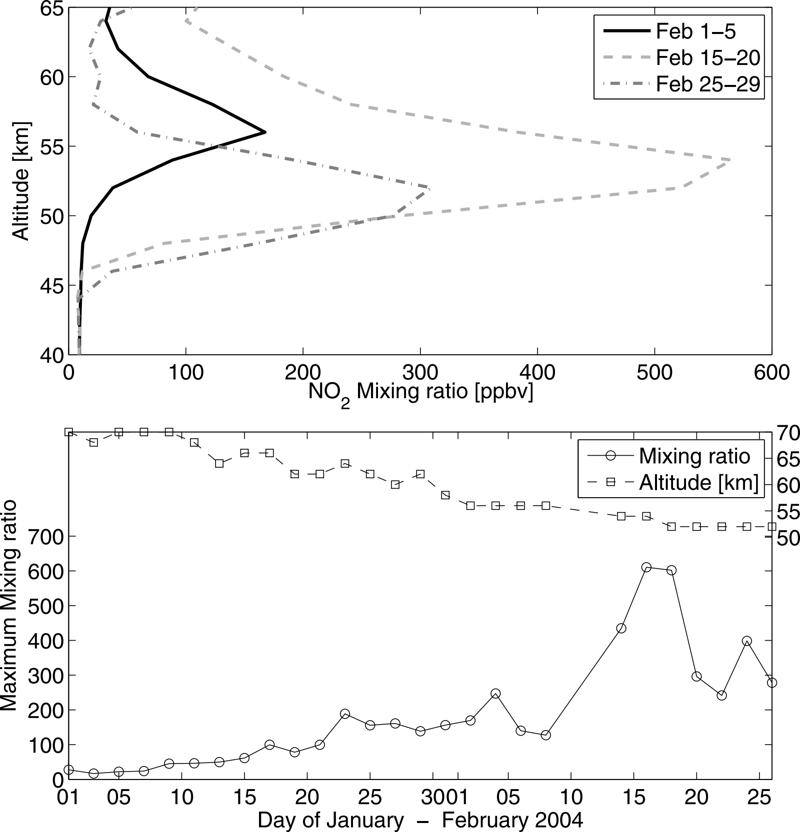
Feb 1−5
Feb 15−20
Feb 25−29
Altitude [km]
NO$_2$ Mixing ratio [ppbv]
Mixing ratio
Altitude [km]
Maximum Mixing ratio
Day of January − February 2004

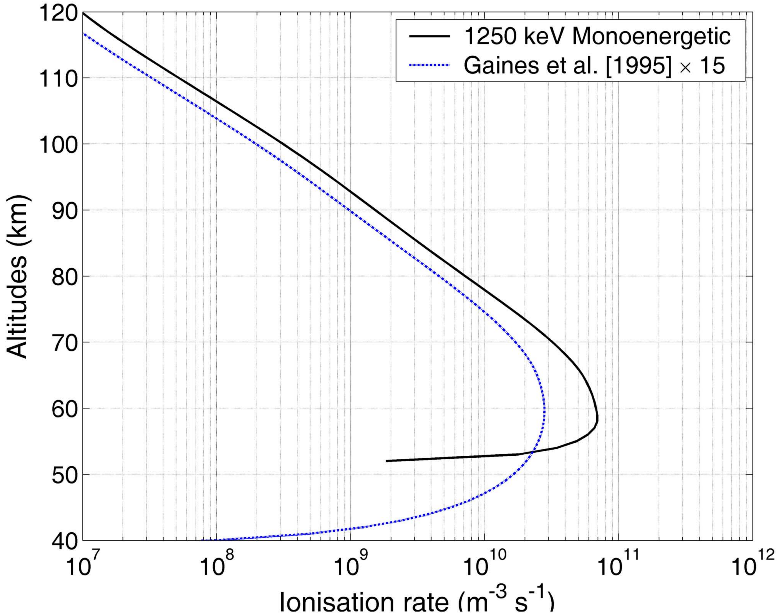

1250 keV Monoenergetic
Gaines et al. [1995] × 15
Altitudes (km)
120
110
100
90
80
70
60
50
40
10^7
10^8
10^9
10^10
10^11
10^12
Ionisation rate (m^-3 s^-1)

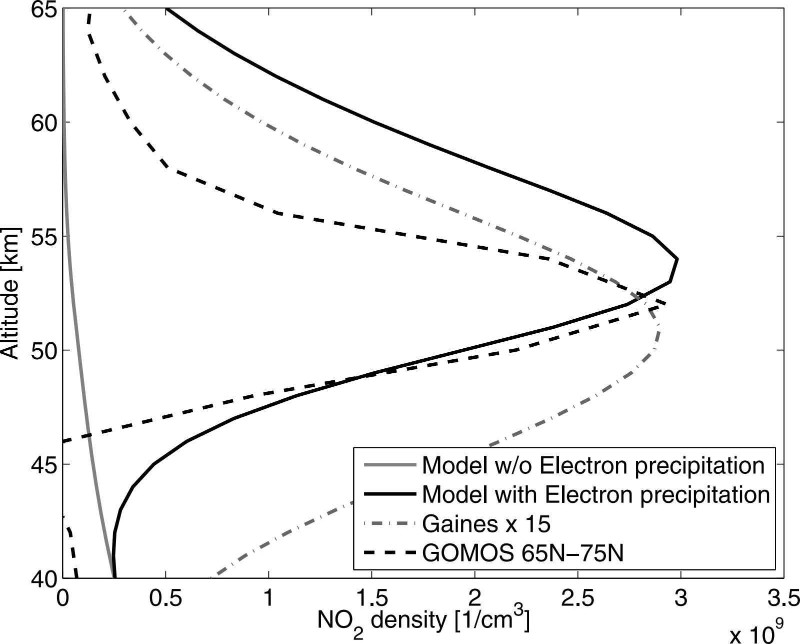

65
60
55
50
45
40
Altitude [km]
0
0.5
1
1.5
2
2.5
3
3.5
NO2 density [1/cm3]
x 10^9
Model w/o Electron precipitation
Model with Electron precipitation
Gaines x 15
GOMOS 65N−75N